Electrical optimization of plasma-enhanced chemical vapor deposition chamber cleaning plasmas

M. A. Sobolewski[a)]
National Institute of Standards and Technology, Gaithersburg, Maryland

J. G. Langan and B. S. Felker
Air Products and Chemicals, Inc., Allentown, Pennsylvania

(Received 23 June 1997; accepted 3 October 1997)

Fluorinated gas discharges are widely used by the semiconductor industry in etching and chamber cleaning applications, but the performance of these discharges varies in unpredictable ways, for unknown reasons believed to be electrical in origin. To investigate possible mechanisms for this behavior, we have measured the electrical characteristics of NF_3/Ar, $CF_4/O_2/Ar$, and $C_2F_6/O_2/Ar$ chamber cleaning plasmas at 6.7–267 Pa in a 13.56 MHz, capacitively coupled, parallel-plate reactor, using radio-frequency current and voltage probes and optical emission spectroscopy. From the measurements, power losses in the external circuitry surrounding the discharge were determined. Furthermore, using the measurements and equivalent circuit models, the mechanisms by which power was absorbed within the discharge itself were investigated. Power was absorbed most efficiently at particular values of the discharge impedance. These optimal impedances occur in the middle of a transition from capacitive impedances at low pressures to resistive impedances at high pressures. These results illustrate that the plasma impedance is a useful parameter for monitoring and optimizing plasma processes in highly electronegative gases. © *1998 American Vacuum Society.* [S0734-211X(98)00101-2]

I. INTRODUCTION

Fluorinated gas discharges are widely used in the semiconductor industry to etch silicon, silicon oxide, and silicon nitride films, and to clean the plasma-enhanced chemical vapor deposition (PECVD) reactors that deposit these films. In PECVD processes, films are deposited not only on the semiconductor substrates—where they are desired—but on all the interior surfaces of the reactor. Deposits on the reactor surfaces must be periodically removed; if the deposits become too thick, they will generate particles that can contaminate the substrates. Fluorinated gas plasmas offer a means of etching away the deposits *in situ*, without disassembling or venting the reactor.

To be commercially successful, any chamber cleaning process must be extremely rapid. Also, there is an increasing desire to minimize the emission of perfluorinated process gases, because they strongly absorb infrared radiation when released to the atmosphere, resulting in an increased greenhouse effect. Unfortunately, optimizing chamber cleaning processes to assure high etch rates and high gas utilization efficiencies can be complicated and time-consuming task. Chamber cleaning performance often varies in unpredictable ways. Since the etching process relies on the reaction of fluorine with silicon, one might expect that the most rapid chamber cleaning would occur at the highest partial pressures of the fluorine-containing feed gas. Previous studies,[1,2] however, have shown that lowering the total pressure or diluting the fluorine-containing species in fluorine-rich plasmas results in faster etch rates. Consequently, local optima in etch rate are observed at intermediate pressures and dilutions.

In this article we investigate the hypothesis that electrical phenomena are responsible for the local optima in etch rate. In particular, the optimization of NF_3/Ar, $CF_4/O_2/Ar$, and $C_2F_6/O_2/Ar$ chamber cleaning plasmas was studied with optical emission spectroscopy and radio-frequency electrical measurements. These measurements enabled a complete determination of power losses in the external circuitry that powers the discharge. Furthermore, using these measurements and simple equivalent circuit models, the mechanisms by which power is dissipated within the discharge itself were investigated. Power losses in the external circuitry were found to be significant, but not critical. The local optima in etch rate were instead explained by the efficiency with which power is used within the discharge itself. This conclusion has important implications for the optimization of chamber cleaning processes and equipment, to be discussed briefly here.

II. EXPERIMENT

Experiments were performed in a gaseous electronics conference (GEC) reference cell,[3] shown in Fig. 1(a). It is a parallel-plate rf system, with an electrode diameter of 10 cm and an electrode separation of 2.3 cm. Both electrodes are surrounded by ground shields. The cell was operated with the top electrode grounded and the bottom electrode powered by a 13.56 MHz generator, coupled through a π-type matching network. Gas entered through a showerhead in the upper electrode. For NF_3/Ar and pure argon discharges, the total flow was maintained at 25 sccm, while the NF_3 flow was varied (0, 2.5, 4.5, 6.25, 9.5, 12.5, and 18.75 sccm). For $C_2F_6/O_2/Ar$ and $CF_4/O_2/Ar$ discharges the total flow was 28 sccm, the argon flow was 3 sccm, and the oxygen flow was

a)Electronic mail: sobo@enh.nist.gov

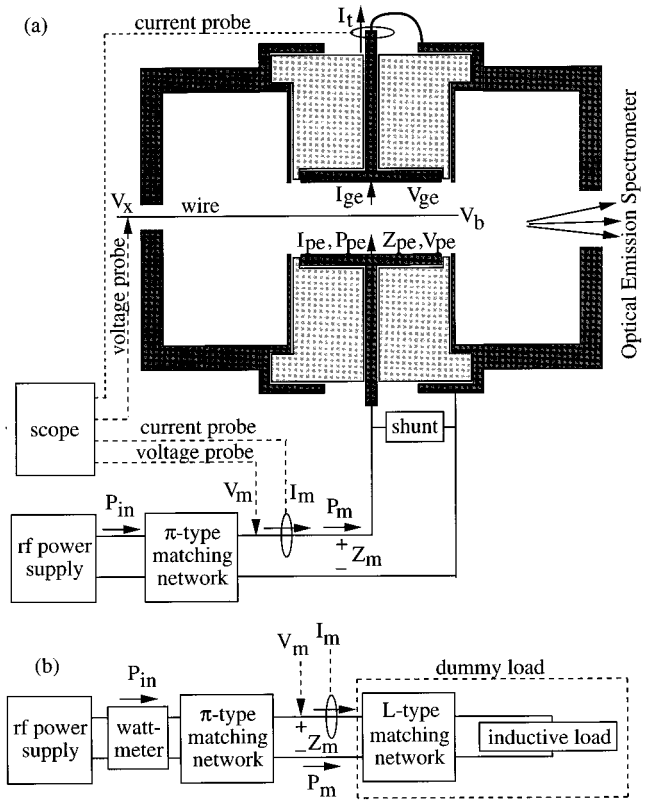

FIG. 1. (a) Diagram of the GEC reference cell showing the placement of the current and voltage probes and the definitions of electrical parameters. (b) Configuration of the power circuitry and the dummy load used to characterize the efficiency of the matching network.

varied (2 and 4 sccm for $CF_4/O_2/Ar$; 12.5 and 18.8 sccm for $C_2F_6/O_2/Ar$). For each mixture, discharges were operated at eight different pressures in the range 67 to 267 Pa (0.05–2.00 Torr), and five different generator powers, from 10 to 50 W.

Probes were mounted at the output of the matching network to measure the current and voltage waveforms there, $I_m(t)$ and $V_m(t)$. The waveforms were digitized by an oscilloscope and transferred to a computer, which determined their complex Fourier components at the fundamental frequency (13.56 MHz), I_m and V_m. Together, I_m and V_m define a complex impedance, $Z_m = V_m/I_m$, which is the combined impedance of everything downstream from the matching network. The phase of Z_m, that is, the phase difference between V_m and I_m, called ϕ_m, was calibrated using loads of known impedance phase and techniques described previously.[4] From V_m, I_m, and ϕ_m we calculated the power flowing at the output of the matching network,

$$P_m = 0.5\, V_m\, I_m \cos\, \phi_m . \tag{1}$$

Fourier components at harmonic frequencies were also recorded, but they are not reported here. No significant power was carried by the harmonic components.

Stray impedances between the matching network and the powered electrode were characterized using open-circuit and short-circuit measurements.[4] (Nearly identical results were obtained with an alternative technique, unterminating and de-embedding.[1]) The characterization allows I_m and V_m to be converted to I_{pe} and V_{pe}, the fundamental components of the current and voltage at the surface of the powered electrode. To improve the precision of this conversion, an inductive shunt circuit[3] was installed in the cell and adjusted to cancel the stray capacitive impedance of the powered electrode assembly at 13.56 MHz. From I_{pe} and V_{pe}, we calculated the impedance $Z_{pe} = V_{pe}/I_{pe}$, which is the combined impedance of everything downstream from the powered electrode, and the power flowing from the powered electrode into the plasma,

$$P_{pe} = 0.5\, V_{pe}\, I_{pe} \cos\, \phi_{pe} . \tag{2}$$

Here, ϕ_{pe} is the phase of Z_{pe}, i.e., the phase difference between V_{pe} and I_{pe}.

A second current probe measured the current at the ground connection of the grounded electrode, $I_t(t)$, and a second voltage probe measured the voltage on a wire probe inserted into the plasma, $V_x(t)$. These signals were digitized by the oscilloscope and their complex Fourier components at the fundamental frequency, I_t and V_x, were obtained. Using procedures described previously,[5] we determined I_{ge} and V_{ge} from I_t, and V_b from V_x. I_{ge} and V_{ge} are the fundamental components of current and voltage on the grounded electrode. V_{ge} is not zero, because the connections that ''ground'' that electrode have a non-negligible impedance at radio frequencies. V_b is the fundamental component of the time-dependent plasma potential in the vicinity of the wire probe. The wire probe consisted of three intertwined wire loops of 0.38 mm diameter steel wire, mounted on a straight support wire. The support wire was attached to an electrical feedthrough mounted on a manipulator attached to a 2.75 in. flange. V_b can be considered a spatial average over a region (roughly 10 cm across and 5 mm thick) defined by the wire loops.

Light emitted from the plasma was collected by an optical emission spectrometer mounted on a 2.75 in. flange. Emission intensity measurements were time averaged and also spatially averaged, since the spectrometer accepted light over a wide range of incident angles. Using a monochrometer, the emission at the fluorine peak at 703.7 nm, as well as other peaks, was monitored. No processing of the optical data was performed, other than a measurement of the peak intensity and a background subtraction.

III. RESULTS

A. Optical emission data

Optical emission measurements were performed in this study because a correlation between fluorine optical emission intensity and the etch rate of silicon oxide and silicon nitride films was previously observed in NF_3/Ar discharges.[2] Examples of this correlation are shown in Fig. 2. The behavior of the oxide etch rate in Fig. 2(a) closely resembles the behavior of the fluorine optical emission intensity in Fig. 2(b). This correlation suggests that the optical emission signal can be used as a predictor of etch rates, and it will be treated as

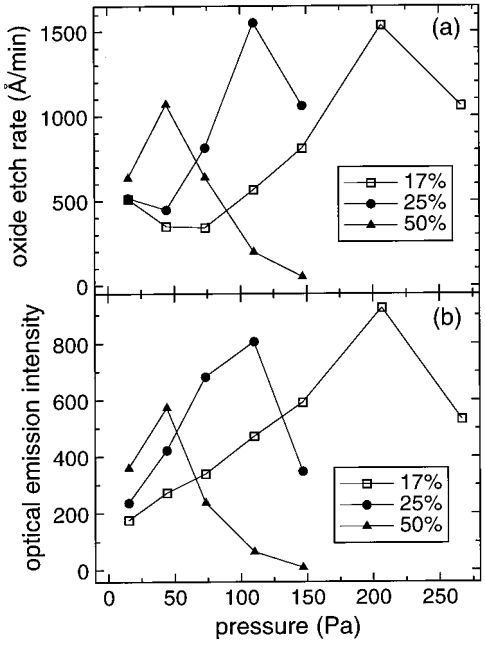

FIG. 2. (a) Measurements of the etch rate of silicon oxide films at varying pressures and concentrations of NF_3 in argon. (b) Intensity of optical emission of the fluorine line at 703.7 nm, in arbitrary units, measured during the oxide etches. The data were not measured in the GEC cell but in another parallel-plate reactor described previously (Ref. 1). Etch rates were measured *in situ* using laser interferometry, for substrates placed on the powered electrode.

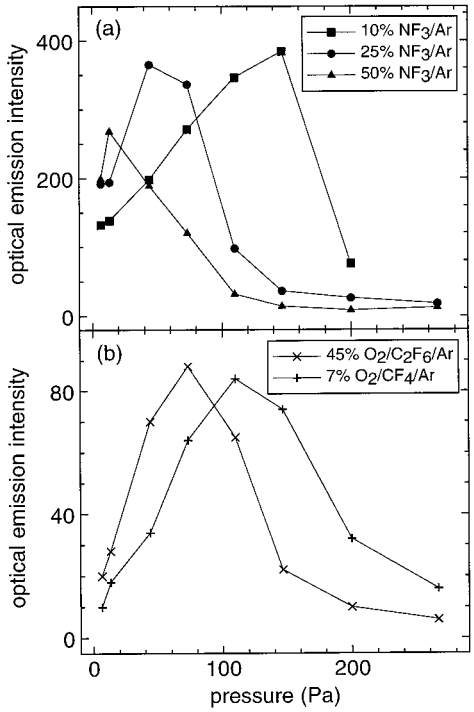

FIG. 3. Optical emission intensity of the fluorine line at 703.7 nm, in arbitrary units, measured in the GEC reference cell, as a function of pressure for (a) mixtures of 10%, 25%, and 50% NF_3 in argon, and (b) a mixture of 7% O_2, 82% CF_4, and 11% Ar, and a mixture of 45% O_2, 45% C_2F_6, and 11% Ar, all at a generator power of 50 W.

such in this article. Etch rate measurements are not included here, but are reserved for future studies of particular ranges identified by the emission measurements as the most promising or interesting.

Figure 3 shows fluorine optical emission intensities measured in this study, in the GEC cell. The results were qualitatively similar to the data in Fig. 2, obtained from a different reactor. For either reactor, at low pressures, the emission intensity increased with pressure or NF_3 concentration. In contrast, at high pressures, emission decreased with pressure or NF_3 concentration. Together, these trends result in local maxima in emission at intermediate pressures. Argon emission signals exhibited similar local maxima.

It is doubtful that a chemical effect could explain the optical data. Electrical explanations seem much more likely. One possible explanation, involving the power coupling efficiency of the external circuitry, is investigated in the next section.

B. Power losses in external circuitry

Although the power measured at the generator is kept constant in Figs. 2 and 3, not all of that power is delivered to the plasma. Part of it is dissipated in external circuitry. Such power losses can be large and variable; reported power coupling efficiencies vary in the range 10%–98%, depending on plasma conditions.[1,6–9] Results describing the efficiency of our system are shown in Fig. 4. In Fig. 4(a), the power at the output of the matching network, P_m, from Eq. (1), differs from the power at the generator (50 W) because of losses in the matching network and further upstream (as well as errors in the generator setpoint). In Fig. 4(b) the power that flows from the powered electrode into the plasma, P_{pe}, obtained from Eq. (2), is further reduced, due to power losses between the matching network and the powered electrode. Overall, the efficiency in Fig. 4(b) ranges from 46% to 81%. Thus, losses in the external circuitry are significant, but they are not large enough to explain the optical emission data. Although local maxima are observed in Fig. 4, they are much less sharp than the peaks in emission intensity in Fig. 3. Furthermore, they do not always occur at the same pressures as the emission maxima.

Presumably, the pressure dependence observed in Fig. 4 results from changes in the efficiency of the matching network as its load impedance, $Z_m = V_m / I_m$, changes with pressure. To verify this, we measured the efficiency of our matching network over a wide range of load impedances. The generator, matching network, and probes were disconnected from the cell and attached to a variable, dummy load which consisted of a second (L-type) matching network and an inductive load, as shown in Fig. 1(b). A wattmeter placed between the rf generator and the matching network measured the net power flowing into the matching network, P_{in}. The power coupling efficiency of the matching network, η_{mn}, is therefore given by the ratio P_m / P_{in}.

To study the dependence of η_{mn} on Z_m, the two variable capacitors in the L-type matching network were varied. After each change in either capacitor, the π-type matching network

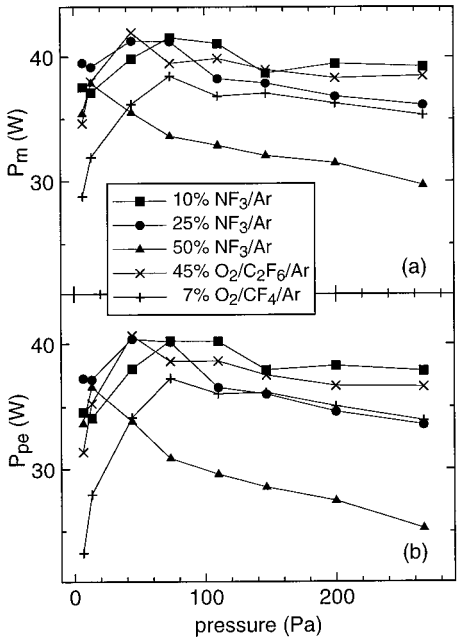

FIG. 4. (a) Power at the matching network output, P_m, and (b) power flowing from the surface of the powered electrode into the discharge, P_{pe}, as a function of pressure, at a generator power of 50 W.

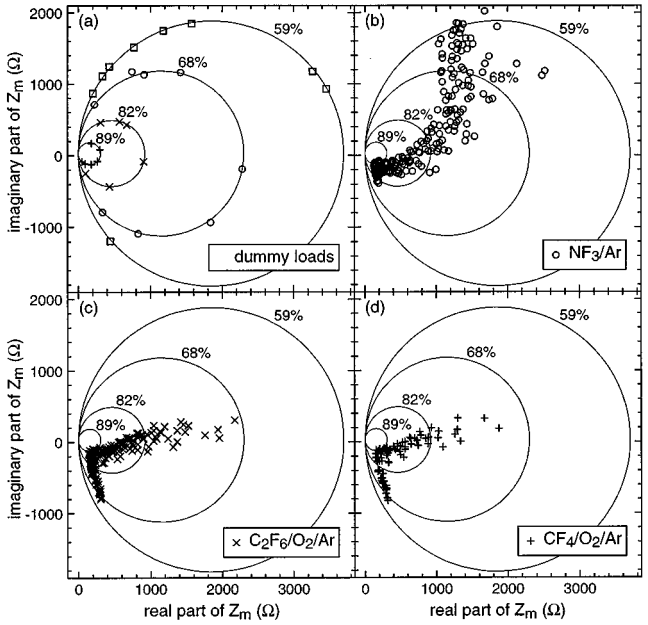

FIG. 5. Complex-plane plots of the impedance at the output of the matching network, Z_m. (a) Values of Z_m measured while operating with the dummy load. The dummy load points fall on circular curves, along which the measured efficiency of the matching network was nearly constant, varying by less than 1% from the values indicated next to each curve. In (b), (c), and (d), values of Z_m measured while operating plasmas are compared to the efficiency contours. (Data from all mixtures, pressures, and generator powers are plotted.)

was tuned to minimize the reflected power measured by the wattmeter. Changes in one capacitor moved the load impedance Z_m along circular paths on the complex plane, shown in Fig. 5(a). The other moved Z_m between the paths. Along the circular paths η_{mn} was found to be constant, within 1%, at the values printed beside each path.

In Figs. 5(b)–5(d) values of Z_m measured with the plasma ignited are plotted. By comparing the position of these points with the circular contours of η_{mn}, one sees that the efficiency of the matching network varied from about 59% to 89% during plasma operation. In general, as the pressure was increased the imaginary part of Z_m became more positive. At low pressures, this trend improves the efficiency, but at high pressures it lowers the efficiency. Thus, the efficiency is maximized at intermediate pressures, as in Fig. 4.

The changes in the impedance Z_m in Fig. 5 are produced by changes in the impedance of the discharge. In addition, the discharge impedance provides information about power losses within the discharge itself. The power P_{pe} is dissipated in the plasma by several competing processes, not all of which produce optical emission or the reactive species necessary for chamber cleaning. Thus, the impedance of the discharge, and the mechanisms by which the discharge dissipates power, are important subjects, to be examined in the remainder of this article.

C. Discharge impedance

The impedance Z_m, shown in Fig. 5, includes the stray impedance of the powered electrode assembly, but the impedance $Z_{pe}=V_{pe}/I_{pe}$ does not. Therefore, Z_{pe} provides a better description of the electrical behavior of the discharge itself. In Fig. 6, Z_{pe} is plotted on the complex plane. In all cases, as the pressure increases, Z_{pe} moves in the direction indicated by the arrows. At the lowest pressures, the imaginary part is large and negative (i.e., capacitive), but it becomes less negative as the pressure is increased. Then the real (resistive) part of Z_{pe} increases, producing a bend in the plot. At the bend, the magnitude of Z_{pe} is minimized, and ϕ_{pe}, the phase of Z_{pe}, is near $-45°$. The bend occurs at pressures of 13–110 Pa, depending on mixture, as shown by the $|Z_{pe}|$ and ϕ_{pe} data in Figs. 7 and 8.

Local maxima in optical emission intensity are observed at the data points circled in Figs. 7 and 8. The emission maxima always occur at or near pressures where $|Z_{pe}|$ is minimized and ϕ_{pe} is $-45°$. These correlations strongly suggest that electrical phenomena are responsible for the maxima in emission intensity. Apparently, the electrical phenomena are quite general, since the correlations were observed for every gas mixture and power we investigated. Furthermore, similar Z_{pe} data have been predicted[10] and observed in other electron-attaching gases, including Cl_2,[10] SF_6,[7,8,11] NF_3,[7] CF_4,[8] and mixtures of Ar with CF_4,[12] C_2F_6,[12] SF_6,[12,13] and CF_3Cl.[14] (Even pure argon discharges exhibit a minimum in $|Z_{pe}|$ at pressures near 270 Pa, the upper limit of this study but well within the pressure range of previous studies.[12,15]) Explanations for this very general behavior are provided by wire probe measurements, discussed in the next section, and equivalent circuit models of the discharge, presented in subsequent sections.

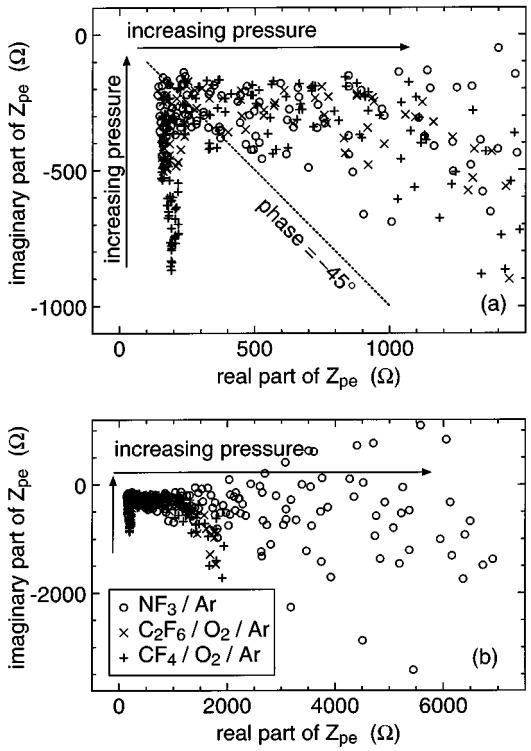

FIG. 6. Plot of the discharge impedance, Z_{pe}, on the complex plane; (a) is a blow-up of the low-impedance region, (b) shows the complete data set. For all mixtures and powers, as the pressure increased, Z_{pe} moved in the directions indicated by the arrows, first vertically upward, then horizontally.

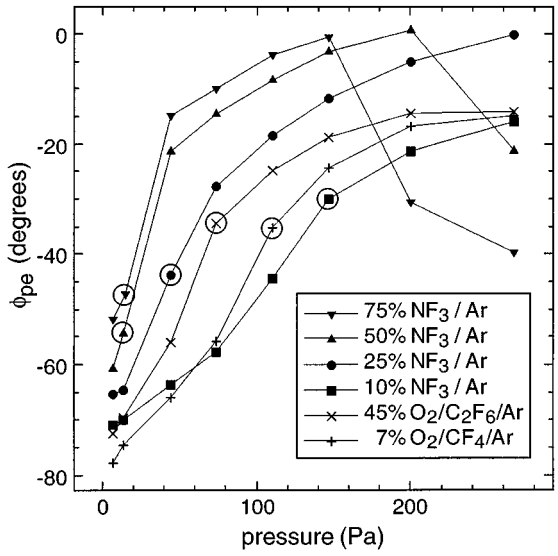

FIG. 8. The phase, ϕ_{pe}, of the discharge impedance, Z_{pe}, as a function of pressure, measured at the same time under the same conditions as the optical emission data in Fig. 3. Circled points coincide with local maxima in the optical emission intensity.

D. Wire probe measurements

Wire probe measurements determine the local rf potential in the plasma in the vicinity of the wire.[5,16] The magnitude of the fundamental component of this potential, V_b, is plotted in Fig. 9(a) as a function of x, the axial position. Also, at the positions corresponding to the ground electrode (0 mm) and the powered electrode (23 mm), the voltages on these electrodes, V_{ge} and V_{pe}, determined from external current and voltage measurements, are shown. Differences between adjacent voltages in Fig. 9(a), including their phases (not shown) were used to estimate the electric field in the x direction, $E_x = -dV/dx$. The magnitude and phase of E_x are shown in Figs. 9(b) and 9(c).

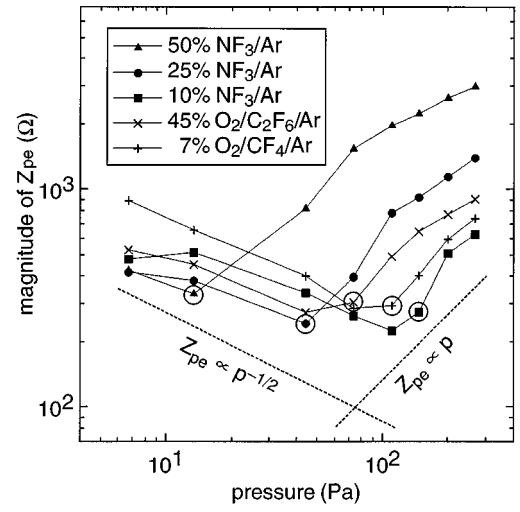

FIG. 7. The magnitude of the discharge impedance, Z_{pe}, as a function of pressure, measured at the same time under the same conditions as the optical emission data in Fig. 3. Circled points coincide with local maxima in the optical emission intensity. Dotted lines show the power law dependences of $|Z_{pe}|$ on pressure, p, predicted by circuit models.

The strong gradients in voltage and high fields near either electrode in Figs. 9(a) and 9(b) indicate the presence of sheaths—regions of relatively low electron density, high space charge density, and high electric field. When the rf frequency is high, a sheath will have a mostly capacitive impedance.[17–20] This is demonstrated by Fig. 9(c), which shows that the phase of E_x in the sheaths approaches the capacitive value, $-90°$. Figure 9(a) shows that the powered electrode sheath has a much larger voltage drop than the ground electrode sheath. Thus, for the conditions shown, the powered electrode sheath has a major influence on the plasma impedance and other electrical properties of the discharge, while the ground electrode sheath makes relatively minor contributions.

For pure argon, in Fig. 9(a), voltage gradients are only seen near the electrodes; none were detected in the middle of the gap. This result agrees with previous studies of argon discharges,[5,12] in which evidence for a bulk electric field in argon has been detected only at pressures $\geqslant 133$ Pa. For the fluorinated gases, however, a gradient in voltage is seen throughout the gap. In the middle of the gap the electric field has a magnitude of roughly 20 V/cm. Figure 9(c) shows that this bulk field is roughly in phase with the current. Therefore the bulk plasma has an impedance that is primarily resistive. Models of this resistance, and of the capacitive impedance of the powered electrode sheath, are presented in the next sec-

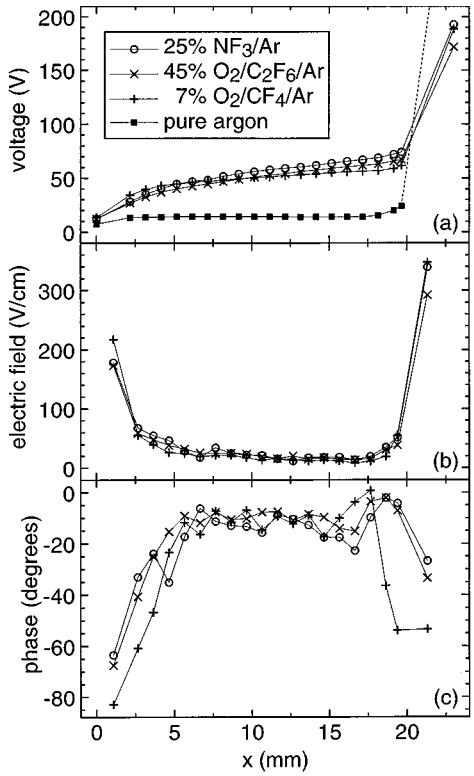

FIG. 9. (a) Capacitive wire probe measurements of the amplitude of the fundamental component of the local rf plasma potential, as a function of the position of the wire probe, x, for several gas mixtures at 73 Pa and a generator power of 50 W. Also plotted are voltages on the ground electrode ($x=0$) and on the powered electrode ($x=23$ mm), determined from external current and voltage probes. The phase of the voltages shown in (a) were also measured but are not shown. (b) Magnitude and (c) phase of the fundamental component of the electric field obtained from the x derivative of the voltages in (a). The phase in (c) is referenced to I_{ge}, the current at the ground electrode.

tion. The models explain why these impedances change with pressure, and how these changes are responsible for the trends seen in Figs. 6–8.

IV. ANALYSIS

A. Simple model of bulk plasma

In a small volume element of plasma, the amplitudes of the current density, j, and the electric field, E, at a given angular frequency, ω, are related by

$$j=\{n_e e^2/[(\nu_e+i\omega)m_e]+i\omega\epsilon_0\}E, \tag{3}$$

where e, m_e, ν_e, and n_e are the charge, mass, collision frequency, and number density of electrons, and ϵ_0 is the permittivity of vacuum. The first term on the right-hand side is the electron conduction current. It describes the Ohmic heating of electrons and their inertia. The second term is the displacement current, which represents the dielectric properties of the bulk plasma. The ion conduction current has been omitted. Because they are so much heavier than electrons, motion of the ions can often be neglected at radio frequencies.

For the weakly ionized plasmas studied here, we expect that electrons collide primarily with neutral gas molecules. Therefore, $\nu_e=u_e N\sigma_e$, where u_e is the mean electron velocity, N is the number density of neutrals, and σ_e is the total cross section for electron-neutral collisions. For electrons at velocities typical for weakly ionized plasmas, on the order of 10^8 cm/s, values of σ_e are on the order of 10^{-15} cm^2 for Ar,[21] CF_4,[22] and C_2F_6.[23,24] Using these estimates, one obtains, at a pressure of 133 Pa, $\nu_e=3.5\times10^9$ s^{-1}, which is much higher than 8.5×10^7 s^{-1}, the value of ω that corresponds to 13.56 MHz. Thus, at 133 Pa, and indeed over all but the lowest pressures studied here, $\nu_e^2\gg\omega^2$, and Eq. (3) reduces to

$$j=[n_e e^2(\nu_e-i\omega)/(m_e\nu_e^2)+i\omega\epsilon_0]E. \tag{4}$$

The impedance of a finite volume of plasma can be obtained by integrating this equation. For a uniform volume of plasma of length L and cross-sectional area A, the current is $I=jA$, the voltage drop is $V_b=EL$, and the impedance Z_b is given by

$$Z_b^{-1}=I/V_b=R_b^{-1}+i\omega C_b-i\omega/(R_b\nu_e), \tag{5}$$

where

$$R_b=\nu_e m_e L/(n_e e^2 A) \tag{6}$$

is a resistance arising from the electron conduction current, $C_b=\epsilon_0 A/L$ is a capacitance arising from the displacement current, and the final, inductive term in Eq. (5) arises from electron inertia. The magnitude and phase of Z_b are

$$|Z_b|=R_b[1+(\omega\nu_e/\omega_e^2-\omega/\nu_e)^2]^{-1/2} \tag{7}$$

and

$$\phi_b=-\text{atan}(\omega\nu_e/\omega_e^2-\omega/\nu_e), \tag{8}$$

where ω_e is the electron plasma frequency,

$$\omega_e=(n_e e^2/m_e\epsilon_0)^{1/2}. \tag{9}$$

The power dissipation in the bulk plasma is

$$\begin{aligned}P_b&=0.5|I||V_b|\cos\phi_b\\&=0.5|I||V_b|[1+(\omega\nu_e/\omega_e^2-\omega/\nu_e)^2]^{-1/2}.\end{aligned} \tag{10}$$

If $\omega^2\nu_e^2/\omega_e^4\ll1$, $\omega^2/\omega_e^2\ll1$, and $\omega^2/\nu_e^2\ll1$, Eqs. (7) and (10) reduce to

$$|Z_b|\approx R_b=\nu_e m_e L/(n_e e^2 A) \tag{11}$$

and

$$P_b\approx0.5|I||V_b|. \tag{12}$$

The validity of these approximations can be verified using the phase data from the bulk region of Fig. 9(c). Substituting the observed phases into Eq. (8) yields $\omega\nu_e/\omega_e^2-\omega/\nu_e\approx1/5$, so that the error in Eqs. (11) and (12) is only 2%.

In Ref. 25, Godyak *et al.* state that the voltage across the bulk plasma (V_b) should be relatively independent of the current (I) because of ionization balance. If V_b is independent of current, then P_b and R_b will obey the scaling laws,

$$P_b\propto|I|\propto1/R_b. \tag{13}$$

B. Model of the powered electrode sheath

The electrical characteristics of radio-frequency plasma sheaths have been widely studied both experimentally[5,25,26] and theoretically,[17–20] especially at high frequencies, where the sheath impedance is primarily capacitive. Lieberman has modeled capacitive sheaths, both at low pressures where ion collisions are negligible[17] and at higher pressures where ion collisions are significant.[18] In the high-pressure regime applicable here, the Lieberman model predicts that the complex impedance of the sheath,

$$Z_s = V_s / I, \tag{14}$$

can be expressed as[20,26]

$$Z_s = -0.80i(e/\omega^5 \epsilon_0^3 A^3 m_i)^{1/5} V_s^{3/5} \lambda_i^{1/5} I_0^{-2/5}, \tag{15}$$

where V_s is the fundamental amplitude of the voltage drop across the sheath; m_i and λ_i are the mass and diffusivity mean free path of ions; and I_0 is the dc ion current. This model, Eq. (15), has been verified for the sheath at the powered electrode of the GEC cell, in argon discharges.[20,26] We expect Eq. (15) to be valid in electronegative discharges as well. Negative ions generated in the glow are repelled by the electric field in the sheath. Since they do not enter the sheath, they do not upset Eq. (15).

From Eqs. (14) and (15) one obtains

$$Z_s = -0.96i(\omega^5 \epsilon_0^3 A^3 m_i / e)^{-1/2} I^{3/2} \lambda_i^{1/2} / I_0. \tag{16}$$

All the factors in this equation are constant, except for I, λ_i, and I_0. Furthermore, the $I^{3/2}$ and I_0 factors tend to cancel each other. For example, measurements of I_0 in argon discharges[26,27] follow a power law dependence, $I_0 \propto I^{1.35}$, nearly independent of pressure. Therefore, the strongest dependence of Z_s is on λ_i. Since λ_i is inversely proportional to pressure, p, Eq. (16) predicts $Z_s \propto p^{-1/2}$. Measurements of the impedance of the powered electrode sheath in argon discharges[5,26] follow this inverse square root dependence. Optical measurements of sheath width also show an inverse square root dependence on pressure.[28] The origin of the $p^{-1/2}$ dependence is revealed by sheath models.[18–20] The increase in the rate of ion collisions at higher pressures hinders the acceleration of ions in the sheath, producing an increase in the ion charge density in the sheath, which, in turn, reduces the sheath width and Z_s.

In contrast, the impedance of the bulk plasma should increase with pressure, because of the ν_e factor in Eq. (11). In the bulk, higher pressure induces more frequent electron collisions and hence produces a higher resistance, R_b. Together, the decrease in Z_s and the increase in R_b with increasing pressure explain the two major trends observed in Fig. 7. At low pressures, where the capacitive impedance of the powered electrode sheath dominates, Z_{pe} decreases roughly as the inverse square root of pressure. At high pressures, where the bulk plasma resistance dominates, Z_{pe} increases roughly linearly with pressure. Because of the n_e factor in Eq. (11), the bulk plasma resistance also depends strongly on gas mixture and generator power. Low powers or strongly attaching gases reduce n_e, thus increasing R_b and shifting the transition from capacitive to resistive behavior to lower pressures.

As the pressure increases, the decrease in Z_s and the increase in R_b cause less of the applied voltage to be dropped across the powered electrode sheath and more to be dropped across the bulk plasma, as observed by wire probe measurements. The rf voltage drop across the sheath, V_s, is partially rectified by the sheath, generating a dc voltage drop, V_{s0}. For large values of V_s, sheath models[17–20] predict

$$V_{s0} \approx V_s. \tag{17}$$

Therefore, V_{s0} should also decline with pressure.

Power is dissipated in the sheath predominantly by ions bombarding the powered electrode. The power dissipated by the ions is

$$P_i = I_0 V_{s0}, \tag{18}$$

which will also decline with pressure, provided that the decrease in V_{s0} is not counteracted by an increase in I_0. Using Eqs. (14)–(18) P_i may be expressed in terms of the rf current.

$$P_i = 0.96(\omega^5 \epsilon_0^3 A^3 m_i / e)^{-1/2} I^{5/2} \lambda_i^{1/2}. \tag{19}$$

The dependence on the dc ion current, I_0, drops out.

C. Power absorbed in the plasma and in the sheath

Using Eqs. (13) and (19) (or equivalent equations presented elsewhere[10,25]) the total power, P_{pe}, can be considered the sum of two power laws of the current, I_{pe}.

$$P_{pe} = k_1 I_{pe} + k_2 I_{pe}^{2.5}, \tag{20}$$

where the factors k_1 and k_2 depend on pressure, but not current. The first term represents the power P_b adsorbed by electrons in the bulk plasma; the second is the power P_i absorbed by ions in the sheath. (The stochastic power dissipation mechanism associated with the boundary between the plasma and the sheath has not been included explicitly, but it has the same current dependence as P_b, so it can be considered to be included in the first term.[25]) The size of each term can be determined by fitting Eq. (20) to P_{pe} vs I_{pe} data, measured at fixed pressure.[25] Equivalent procedures that fit resistances rather than the power P_{pe} have also been used.[5,25,29] Here, we use a different procedure, based on the log–log derivative,

$$\zeta \equiv \partial \ln P_{pe} / \partial \ln I_{pe} = I_{pe} \partial P_{pe} / P_{pe} \partial I_{pe}. \tag{21}$$

If power is dissipated entirely by ions in the sheath, $\zeta = 2.5$. If power is dissipated entirely by electrons in the bulk plasma, $\zeta = 1.0$. If power is dissipated by both mechanisms, an intermediate value of ζ will be observed. The fraction of the power dissipated by each mechanism can be obtained by solving Eq. (20) simultaneously with its derivative

$$\partial P_{pe} / \partial I_{pe} = k_1 + 2.5 k_2 I_{pe}^{1.5}. \tag{22}$$

The fraction of the power dissipated by ions is

$$k_2 I_{pe}^{2.5} / P_{pe} = 2(\zeta - 1)/3. \tag{23}$$

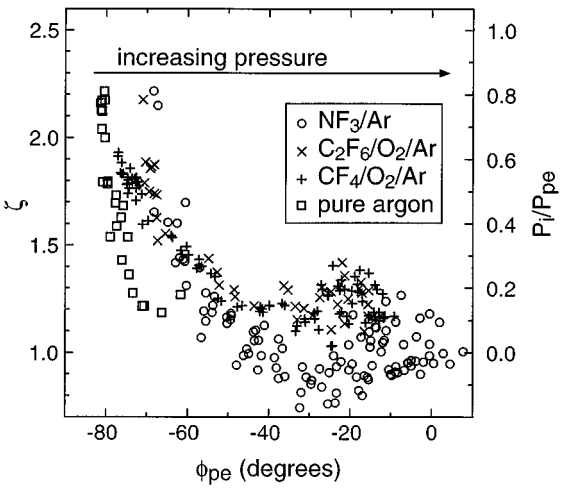

FIG. 10. Plot of ζ, the log–log derivative of discharge power P_{pe} with respect to discharge current I_{pe}, defined by Eq. (21). A linear transform of ζ, given in Eq. (23), yields the fraction of the discharge power dissipated by ion bombardment, P_i/P_{pe}, plotted on the right-hand scale. The x axis is ϕ_{pe}, the phase of the discharge impedance Z_{pe}. Since the phase generally becomes more resistive at higher pressures, data points at low pressures appear towards the left, at negative phases; data points at high pressures appear on the right.

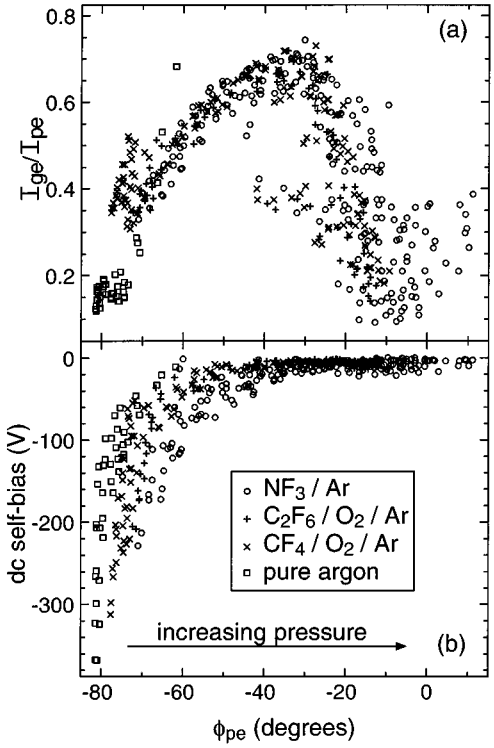

FIG. 11. (a) Ratio of the amplitudes of the fundamental components of current at the ground electrode (I_{ge}) and the current at the powered electrode (I_{pe}) and (b) the dc self-bias on the powered electrode, as a function of ϕ_{pe}, the phase of the discharge impedance Z_{pe}. Since the phase generally becomes more resistive at higher pressures, the arrow indicates the direction of increasing pressure. Data from all mixtures, pressures, and generator powers are shown.

By taking differences between values of P_{pe} and I_{pe} measured at varying generator powers, with all other experimental parameters held constant, estimates for ζ were obtained. They are plotted in Fig. 10. At low pressures, when the phase ϕ_{pe} is capacitive and the sheath voltage is large, ζ is close to 2.5. As the pressure increases and ϕ_{pe} becomes more resistive, ζ decreases, indicating a decrease in the fraction of the power absorbed by ions in the sheath and an increase in the fraction absorbed by electrons in the bulk. Presumably, it is the power absorbed in the bulk plasma that accelerates the energetic electrons that are needed to excite states that will emit light. The energy gained by ions in the sheath does not produce emission; it is dissipated as heat when they strike the electrode. Thus the change in the power absorption mechanisms with pressure in Fig. 10 explains the rise in the optical emission intensity with increasing pressure, observed at low pressures in Figs. 2 and 3. Since energetic electrons are also needed to generate chemically reactive species, the etch rate for etching processes that are purely chemical in nature should also increase with pressure at low pressures, as observed in Fig. 2(a). At higher pressures, however, the emission intensity and etch rate fall with pressure. This reversal is apparently related to a ''collapse'' of the discharge observed at high pressures, described in the next section.

V. COLLAPSE OF THE DISCHARGE

The models used above assume that the discharge is uniform, but at high pressures the discharge becomes extremely nonuniform. This nonuniformity is evidenced by a dramatic contraction in the glow which is visible to the eye and has also been studied in detail with spatially resolved planar laser-induced fluorescence and optical emission.[30] At low pressures the glow may be observed far into remote regions near the chamber walls, but as the pressure increases the glow becomes more confined within the interelectrode gap. Then the glow appears to contract towards the powered electrode—a bright glow is observed in its vicinity, and only a much fainter glow is observed near the ground electrode. Finally, the bright glow collapses to a thin ring (or a double ring or a broken ring) between the powered electrode and its ground shield. The rest of the gap glows very dimly or not at all.

Wire probe measurements show that the electric field in dimly glowing regions has a phase that is predominantly capacitive but the field in the bright glow is predominantly resistive. Therefore, from Eqs. (8) and (9), the bright glow has a higher value of ω_e, and hence a higher electron density, than the dimly glowing region. Thus, as the pressure increases, a contraction of the electron density accompanies the contraction of the glow. In contrast, the dim, low-density, capacitive region near the ground electrode expands; this expansion is responsible for the trend towards capacitive phases observed for some data points at high pressures in Figs. 6 and 8.

The current density, too, becomes confined to a smaller and smaller volume as the pressure increases. This is illustrated in Fig. 11(a), which plots I_{ge}/I_{pe}, the fraction of the

current flowing to the ground electrode. At low pressures, when the bright glow extends far outside the interelectrode gap, I_{ge}/I_{pe} is small because a large fraction of the current flows out to the chamber walls. Under these circumstances, the ''effective'' grounded area of the cell is large, the current density at the grounded surfaces is small, and the rf and dc voltage drops across the sheath at the grounded surfaces are much smaller than the drops across the powered electrode sheath. Therefore, a large, negative dc self-bias is measured on the powered electrode [see Fig. 11(b)]. As the pressure is increased, the glow recedes from the chamber wall, the wall current decreases, and I_{ge}/I_{pe} increases. When $I_{ge} \approx I_{pe}$, the powered electrode and ground electrode sheaths have nearly equal current densities and sheath voltages, so the dc bias approaches zero. In contrast, at higher pressures, as the glow starts to recede from the ground electrode and collapse to a ring, I_{ge}/I_{pe} decreases, presumably because a greater fraction of I_{pe} is flowing directly from the powered electrode to its ground shield. This, apparently, is also a rather symmetric situation, as the dc bias remains close to zero.

Thus, as the pressure increases, we observe that a region of high optical emission intensity, electron density, and current density becomes increasingly confined to the neighborhood of the powered electrode. One explanation for this collapse is provided by Paranjpe *et al.*,[31] who note that, in electronegative discharges, the ionization rate will exceed the attachment rate only if the electric field is above a critical value. As the pressure increases, the critical field increases, and, in remote parts of the chamber where the fields are below the critical field, ionization should be increasingly dominated by attachment.

The collapse can also be explained by impedance arguments. At high pressures, the resistance of the bulk plasma is the dominant impedance, and Eq. (13) predicts that this resistance decreases as the current increases (because additional current will produce additional ionization and hence increase the plasma density). Therefore, if the current taking one path through the plasma increases, the resistance of this path will decrease, causing it to draw additional current at the expense of other current paths. Thus the plasma resistance provides a positive feedback mechanism that eventually results in the collapse of the discharge. In contrast, the impedance of the sheath in Eq. (16) *increases* with current. An increase in the current density through any small area of the electrode will result in an increase in the local sheath impedance, which will oppose any additional increase in the local current density. Thus the sheath provides a negative feedback mechanism that acts to prevent the collapse of the discharge, especially at low pressures where the sheath impedance dominates. Because these arguments are based on general principles, we believe the collapse of the discharge to be a general phenomenon, not limited to the particular cell geometry studied here. Indeed, even in cells that do not have ground shields, we have observed glows collapsing at high pressures, towards closely spaced points on the backside of the powered electrode or on the power feedthrough.

As the brightly glowing plasma collapses and forms a ring discharge, its emission is less efficiently coupled into the spectrometer. Thus the collapse contributes to the decline in optical emission intensity at high pressures in Figs. 2 and 3. Presumably, the ionization rate and the production of reactive species are also higher in the bright region, so these processes also become more localized to the edge of the powered electrode as the pressure increases. In the collapsed discharges, a large fraction of the feed gas may exit the reactor without ever having entered the small, intensely glowing region, so it could well be that collapsed, high-pressure discharges are inherently less efficient at generating reactive species than discharges at intermediate pressures, which occupy larger volumes. Indeed, a mass spectrometer recently installed in the exhaust line of the cell has demonstrated that the decomposition of feed gases is largest at intermediate pressures where I_{ge}/I_{pe} is maximized.[32] Also, species that are generated in high-pressure collapsed discharges are not efficiently transported to the center of the electrode.[30] Thus, the collapse of the discharge explains the decline in etch rate at high pressures in Fig. 2.

Other mechanisms may also reduce the efficiency of the generation of reactive species at high pressures. First, for high-pressure, highly electronegative conditions, absorption of power by ions in the *plasma*—ignored here—may be significant. Indeed, impedances with inductive phases, observed for some data points at high pressures in Fig. 6, may be an indication of ionic conduction. Second, it is conceivable that, in high-pressure sheaths, a new power dissipation mechanism operates, with the observed power law exponent, $\zeta \approx 1.0$, rather than the value $\zeta = 2.5$ predicted in Sec. IV B. In particular, in collapsed discharges, the current density in the powered electrode sheath should vary widely from the edge to the center of the electrode. Under these conditions, the sheath area, A, in Eq. (19) should perhaps not be considered as the total electrode area but as an ''effective area,'' i.e., the area of the region of high current density near the rim of the electrode. A linear dependence of the effective sheath area on sheath current, inserted into Eq. (19), would yield $\zeta \approx 1.0$. For such a sheath, the conclusion made above, that sheath power can be neglected at high pressures, would not necessarily apply.

VI. CONCLUSIONS

In this article, a detailed study of the power dissipation mechanisms in fluorinated gas discharges was presented. Power losses in the cell parasitics and the external circuitry were found to be rather constant and relatively unimportant. In contrast, the efficiency with which power is absorbed within the discharge itself was identified as a critical concern.

Two different regimes of discharge electrical behavior were observed. First, there is a capacitive regime at low pressures in which the discharge impedance is dominated by the sheath at the powered electrode. In the capacitive regime, increasing the pressure produces a decrease in the width and capacitive impedance of the sheath at the powered electrode, and in the dc and rf voltages across it. The power absorbed

by ions in the sheath, which is dissipated at the powered electrode, also decreases with increasing pressure. This makes more power available to be absorbed by electrons in the plasma, producing more ionization, more emission, and more production of the reactive species necessary for chamber cleaning.

In the second regime, at higher pressures, the discharge impedance is dominated by the bulk plasma resistance, which increases with pressure. At high pressures, the discharge collapses to a small volume between the powered electrode and its ground shield. The collapsed discharges are less efficient than larger, more uniform discharges at generating reactive species and transporting them to cell surfaces.

Optical emission data and etch rate measurements suggest that the best operating point for chamber cleaning is near the transition between the two regimes. The transition occurred at pressures that varied from 13 to 110 Pa, increasing with rf power and decreasing as the gas mixture becomes more electronegative. Nevertheless, in all cases, at the transition point, the magnitude of the discharge impedance Z_{pe} is minimized and its phase is near $-45°$. Thus, monitoring the magnitude and/or phase of Z_{pe} may make it easier to find and maintain optimal operating conditions for chamber cleaning.

The plasma impedance measurements presented here may also aid in the scaling of commercial reactors and the design of the electrical systems that power them. For example, deposition chambers designed for 300 mm diameter wafers will have electrode areas roughly nine times larger than the GEC cell. Optimized chamber cleaning plasmas in these reactors should therefore have impedances that are roughly one-ninth of the optimal values of Z_{pe} measured here. Specifically, we expect impedances in the range: $20\,\Omega \leqslant \mathrm{Re}(Z_{\mathrm{pe}}) \leqslant 40\,\Omega$ and $-15\,\Omega \leqslant \mathrm{Im}(Z_{\mathrm{pe}}) \leqslant -30\,\Omega$. Furthermore, if the 300 mm chamber has a parasitic shunt capacitance of 500 pF, a typical value for commercial reactors, we would expect that $3.5\,\Omega \leqslant \mathrm{Re}(Z_m) \leqslant 7.5\,\Omega$ and $-10\,\Omega \leqslant \mathrm{Im}(Z_m) \leqslant -15\,\Omega$. To optimize the performance of such a reactor, a matching network should be selected that operates efficiently in this range of load impedances.

The electrical phenomena observed here appear to be quite general. For every gas mixture and power we investigated, both regimes of electrical behavior were observed. Indeed, similar electrical data have been reported in many other gases.[7,8,10–15] Furthermore, the equivalent-circuit models presented here show that the observed electrical behavior follows from very general principles. Nevertheless, to determine exactly how far the results of this work may be generalized, measurements at higher power levels and in cell geometries that more closely resemble commercial deposition reactors may be needed. Detailed studies of the etch rates on different cell surfaces are also an important area for future study. Finally, measurements of the utilization efficiency of the process gases and the composition and environmental impact of effluent gases would be needed to optimize these aspects of chamber cleaning. Although some of these are primarily chemical, not electrical, issues, the work presented here may serve to assist future studies of such issues, by restricting the parameter space that needs to be evaluated. Also, by allowing electrical effects to be distinguished more easily from purely chemical effects, this work also provides a firmer foundation and a better-defined basis of comparison for future studies of plasma chemistry.

[1] J. G. Langan, S. E. Beck, B. S. Felker, and S. W. Rynders, J. Appl. Phys. **79**, 3886 (1996).
[2] J. G. Langan, B. S. Felker, S. W. Rynders, and S. E. Beck (unpublished).
[3] P. J. Hargis, Jr., K. E. Greenberg, P. A. Miller, J. B. Gerardo, J. R. Torczynski, M. E. Riley, G. A. Hebner, J. R. Roberts, J. K. Olthoff, J. R. Whetstone, R. J. Van Brunt, M. A. Sobolewski, H. M. Anderson, M. P. Splichal, J. L. Mock, P. Bletzinger, A. Garscadden, R. A. Gottscho, G. Selwyn, M. Dalvie, J. E. Heidenreich, J. W. Butterbaugh, M. L. Brake, M. L. Passow, J. Pender, A. Lujan, M. E. Elta, D. B. Graves, H. H. Sawin, M. J. Kushner, J. T. Verdeyen, R. Horwath, and T. R. Turner, Rev. Sci. Instrum. **65**, 140 (1994).
[4] M. A. Sobolewski, J. Vac. Sci. Technol. A **10**, 3550 (1992).
[5] M. A. Sobolewski, IEEE Trans. Plasma Sci. **23**, 1006 (1995).
[6] F. Bose, R. Patrick, and H. P. Baltes, J. Vac. Sci. Technol. B **12**, 2805 (1994).
[7] B. Andries, G. Ravel, and L. Peccoud, J. Vac. Sci. Technol. A **7**, 2774 (1989). [The parallel resistances and reactances reported in this article must be transformed to the series resistance and reactance, $\mathrm{Re}(Z_{\mathrm{pe}})$ and $\mathrm{Im}(Z_{\mathrm{pe}})$, before making comparisons.]
[8] J. W. Butterbaugh, L. D. Baston, and H. H. Sawin, J. Vac. Sci. Technol. A **8**, 916 (1990).
[9] S. E. Savas, D. E. Horne, and R. W. Sadowski, Rev. Sci. Instrum. **57**, 1248 (1986).
[10] Y. T. Lee, M. A. Lieberman, A. J. Lichtenberg, F. Bose, H. Baltes, and R. Patrick, J. Vac. Sci. Technol. A **15**, 113 (1997).
[11] R. Foest, J. K. Olthoff, R. J. Van Brunt, E. C. Benck, and J. R. Roberts, Phys. Rev. E **54**, 1876 (1996).
[12] P. Bletzinger, J. Appl. Phys. **67**, 130 (1990).
[13] B. E. Thompson and H. H. Sawin, J. Electrochem. Soc. **133**, 1887 (1986).
[14] K. D. Allen, H. H. Sawin, M. T. Mocella, and M. W. Jenkins, J. Electrochem. Soc. **133**, 2315 (1986).
[15] P. Bletzinger and M. J. Fleming, J. Appl. Phys. **62**, 4688 (1987).
[16] V. A. Godyak and R. B. Piejak, J. Appl. Phys. **68**, 3157 (1990).
[17] M. A. Lieberman, IEEE Trans. Plasma Sci. **16**, 638 (1988).
[18] M. A. Lieberman, IEEE Trans. Plasma Sci. **17**, 338 (1989).
[19] V. A. Godyak and N. Sternberg, Phys. Rev. A **42**, 2299 (1990).
[20] M. A. Sobolewski, Phys. Rev. E **56**, 1001 (1997).
[21] B. Chapman, *Glow Discharge Processes* (Wiley, New York, 1980).
[22] L. G. Christophorou, J. K. Olthoff, and M. V. V. S. Rao, J. Phys. Chem. Ref. Data **25**, 1341 (1996).
[23] J. Sanabia and J. H. Moore (private communication).
[24] L. G. Christophorou and J. K. Olthoff, J. Phys. Chem. Ref. Data **27**, 1 (1998).
[25] V. A. Godyak, R. B. Piejak, and B. M. Alexandrovich, IEEE Trans. Plasma Sci. **19**, 660 (1991).
[26] M. A. Sobolewski, Appl. Phys. Lett. **70**, 1049 (1997).
[27] V. A. Godyak, R. B. Piejak, and B. M. Alexandrovich, J. Appl. Phys. **69**, 3455 (1991).
[28] N. Mutsukura, K. Kobayashi, and Y. Machi, J. Appl. Phys. **68**, 2657 (1990).
[29] L. J. Overzet and F. Y. Leong-Rousey, Plasma Sources Sci. Technol. **4**, 432 (1995).
[30] K. L. Steffens and M. A. Sobolewski, in Proceedings of the American Vacuum Society 44th National Symposium, San Jose, 1997 (unpublished).
[31] A. P. Paranjpe, J. P. McVittie, and S. A. Self, J. Vac. Sci. Technol. A **8**, 1654 (1990).
[32] W. R. Entley, J. G. Langan, B. S. Felker, and M. A. Sobolewski, in Proceedings of the American Vacuum Society 44th National Symposium, San Jose, 1997 (unpublished).